

Small, Thin Graphene Oxide Is Anti-inflammatory Activating Nuclear Factor Erythroid 2-Related Factor 2 *via* Metabolic Reprogramming

Christopher Hoyle,[†] Jack Rivers-Auty,[†] Eloïse Lemarchand,[†] Sandra Vranic,^{‡,§} Emily Wang,[†] Maurizio Buggio,^{‡,§} Nancy J. Rothwell,[†] Stuart M. Allan,[†] Kostas Kostarelos,^{‡,§} and David Brough^{*,†,§}

[†]Division of Neuroscience and Experimental Psychology, School of Biological Sciences, Faculty of Biology, Medicine and Health, Manchester Academic Health Science Centre, University of Manchester, AV Hill Building, Oxford Road, Manchester M13 9PT, United Kingdom

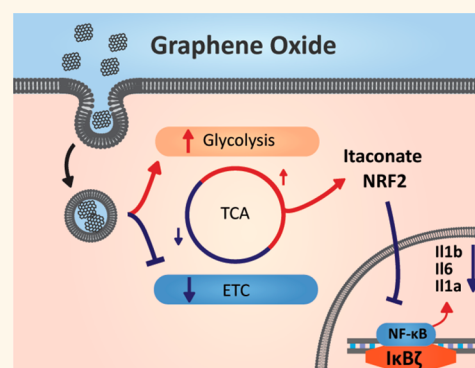
[‡]Nanomedicine Lab, Faculty of Biology, Medicine and Health, University of Manchester, AV Hill Building, Oxford Road, Manchester M13 9PT, United Kingdom

[§]National Graphene Institute, University of Manchester, Booth Street East, Manchester M13 9PL, United Kingdom

Supporting Information

ABSTRACT: Graphene oxide (GO), an oxidized form of graphene, has potential applications in biomedical research. However, how GO interacts with biological systems, including the innate immune system, is poorly understood. Here, we elucidate the effects of GO sheets on macrophages, identifying distinctive effects of GO on the inflammatory phenotype. Small, thin (s)-GO dose-dependently inhibited release of interleukin (IL)-1 β and IL-6 but not tumor necrosis factor α . NLRP3 inflammasome and caspase-1 activation was not affected. The effect of s-GO was pretranslational, as s-GO blocked Toll-like receptor 4-dependent expression of *Il1b* and *Il6* but not *Nlrp3* or *Tnf* mRNA transcripts. s-GO was internalized by immortalized bone-marrow-derived macrophages, suggesting a potential intracellular action. Uptake of polystyrene beads with similar lateral dimensions and surface charge did not phenocopy the effects of s-GO, suggesting that s-GO-mediated inhibition of interleukin expression was not simply due to particle phagocytosis. RNA-Seq analysis established that s-GO had profound effects on the immunometabolism of the cells, leading to activation of the transcription factor nuclear factor erythroid 2-related factor 2, which inhibited expression of cytokines such as IL-1 β and IL-6. Thus, we have identified immunometabolic effects of GO that reveal another dimension to its effects on cells. These findings suggest that s-GO may be used as a valuable tool to generate further insights into inflammatory mechanisms and indicate its potential applications in biomedicine.

KEYWORDS: graphene oxide, macrophage, inflammation, inflammasome, NLRP3, IL-1 β , immunometabolism



that s-GO had profound effects on the immunometabolism of the cells, leading to activation of the transcription factor nuclear factor erythroid 2-related factor 2, which inhibited expression of cytokines such as IL-1 β and IL-6. Thus, we have identified immunometabolic effects of GO that reveal another dimension to its effects on cells. These findings suggest that s-GO may be used as a valuable tool to generate further insights into inflammatory mechanisms and indicate its potential applications in biomedicine.

Graphene is a two-dimensional nanomaterial that is derived from graphite and consists of a single layer of sp² carbon atoms organized in a hexagonal lattice structure.¹ Graphene oxide (GO) is a derivative of graphene that possesses oxygen-containing functional groups on its surface, improving its colloidal properties and allowing a more stable dispersion in aqueous media.² GO has promise as a tool for use in biological applications, such as bioimaging, biosensing, drug delivery, and tissue engineering.^{3–6} Thus, it is important to understand the interactions of GO with major biological systems. In particular, the particle-like properties of

GO make it a likely candidate to interact with innate immune cells and subsequently influence inflammatory responses.

Inflammation is an important component of the innate immune system, promoting pathogen clearance and host survival after infection. However, the innate immune system can also detect markers of cellular damage or stress that occur in the absence of infection and trigger an inflammatory

Received: May 15, 2018

Accepted: November 16, 2018

Published: November 16, 2018

Table 1. Full Physicochemical Analysis and Characterization of l-GO, s-GO, and us-GO Materials Used^a

parameter	technique	l-GO	s-GO	us-GO
lateral dimension	optical microscopy	1 μm to 32 μm		
	AFM	5–20 μm	30–700 nm	30–300 nm
	TEM	0.5–15 μm	50 nm to 3 μm	20–200 nm
thickness	AFM	1 nm–5 nm	1–7 nm	1–4 nm
degree of defects $I(D)/I(G)$	Raman	1.30 \pm 0.09	1.35 \pm 0.03	1.34 \pm 0.03
surface charge	ζ -potential	–61.7 \pm 1.8 mV	–55.0 \pm 0.8 mV	–34.8 \pm 0.1 mV
functionalization degree	TGA	37%	39%	37%
chemical composition	XPS	C, 68.3%; O, 31.5%; N, 0.3%	C, 67.8%; O, 31.8%; N, 0.4%; Na, 0.1%	C, 68.4%; O, 31.0%; N, 0.4%; Na, 0.3%
purity (C/O ratio)	XPS	99.7% (2.2)	99.5% (2.1)	99.4% (2.2)
π - π^* , O=C–O, C=O, C–O, C–C, and C=C	XPS	1.3%, 16.8%, 33.1%, 10.1%, 38.7%	1.3%, 15.1%, 31.2%, 12.7%, 39.8%	1.7%, 15.4%, 28.9%, 9.6%, 44.4%

^aAbbreviations: AFM, atomic force microscopy; TEM, transmission electron microscopy; TGA, thermogravimetric analysis; XPS, X-ray photoelectron spectroscopy.

response.⁷ Inflammation is increasingly implicated in the pathophysiology of many diseases, including cancer, obesity, diabetes, Alzheimer's disease, and stroke.^{8–11}

Innate immune cells, including macrophages and neutrophils, express pattern recognition receptors (PRRs) that respond to specific pathogen-derived motifs or signals of cellular stress or death derived from the host, termed pathogen-associated molecular patterns (PAMPs) and damage-associated molecular patterns (DAMPs), respectively. PRRs can be simplistically divided into membrane-bound and soluble.¹² Membrane-bound PRRs, which include the Toll-like receptor (TLR) family, survey the extracellular or vesicle lumen space for PAMPs and DAMPs, whereas soluble PRRs monitor the cytosolic compartment. Some soluble PRRs form oligomeric protein complexes called inflammasomes, which are responsible for the regulation of pro-inflammatory responses upon detection of infection or injury.¹³ These inflammasome-forming PRRs include NACHT, LRR, and PYD domain-containing protein 3 (NLRP3), NLRP1, NLR and caspase activation and recruitment domain-containing 4 (NLRC4), absent in melanoma 2 (AIM2) and pyrin.^{13–17} NLRP3 is a key regulator of sterile (non-infectious) inflammation and therefore represents a major therapeutic target.

Basal NLRP3 expression in resting cells is not sufficient to form active inflammasomes in response to infection or damage without an initial priming step.¹⁸ Priming typically occurs through membrane-bound PRRs, which detect PAMPs or DAMPs. An example of a commonly studied PAMP is lipopolysaccharide (LPS), which activates the PRR TLR4.¹⁹ This in turn leads to the generation of intracellular signaling cascades, eventually causing the nuclear accumulation of the transcription factor nuclear factor (NF)- κ B, where it drives inflammatory gene expression.²⁰ NF- κ B-dependent genes include *Nlrp3*, *Il1b*, *Tnf*, and *Il6*.^{21–24} The NLRP3 protein must be licensed prior to activation through post-translational deubiquitination and phosphorylation.^{25–28} Following priming, NLRP3 is activated in response to detection of a further PAMP or DAMP stimulus. PAMPs include nigericin (a K⁺ ionophore), whereas examples of DAMPs are extracellular adenosine triphosphate (ATP) acting *via* the P2X7 receptor, aggregated amyloid- β , and crystals of monosodium urate.^{29–31}

Once activated, NLRP3 interacts with an adaptor protein called apoptosis-associated speck-like protein containing a caspase recruitment domain (ASC). The ASC molecules

within the cell then nucleate to form a speck, which serves as a platform for recruitment of pro-caspase-1, facilitating its proximity-induced autocleavage and activation.³² Caspase-1 processes the inactive precursor of interleukin (IL)-1 β , pro-IL-1 β , into its active pro-inflammatory secreted form.³³ Although the mechanism of IL-1 β release from macrophages is unclear, it may be dependent upon a hyperpermeable membrane.^{34,35}

This study aimed to test the effects of different lateral dimension GO sheets (small (s-), ultrasmall (us-), and large (l-)) on inflammasome responses in macrophages. We report that s-GO had a profound effect on the immunometabolism of the cell, leading to altered cytokine production in response to an inflammatory challenge. These insights reveal important information about the effects of GO within cells and indicate its potential applications in biomedicine.

RESULTS

Synthesis and Characterization of GO Sheets. A modified Hummers method optimized for biological investigations (see [Methods](#)) was used to synthesize thin l-, s-, and us-GO sheets. The GO suspensions in water-based solutions were homogeneous, of brownish color, and stable at room temperature for at least 6 months. The detailed description of the synthesis, purification, and physicochemical characterization of all three types of GO sheets used in this study have been recently reported elsewhere³⁶ and are summarized in [Table 1](#). Lateral dimensions of l-, s-, and us-GO sheets are distributed between 0.5–32 μm , 30 nm and 3 μm , and 20–300 nm, respectively. The structural description of the GO sheets was studied using atomic force microscopy (AFM) ([Figure S1](#)). Thickness of the sheets was found to be between 1 and 5 nm for l-GO, 1 and 7 nm for s-GO, and 1 and 4 nm for us-GO ([Table 1](#) and [Figure S1](#)). Materials were tested for endotoxin contamination as previously reported³⁷ and were all found to be endotoxin-free before any further study was performed.

s-GO Inhibits NLRP3 Inflammasome-Dependent IL-1 β Release. To evaluate the effect of s-GO on NLRP3 inflammasome activation and IL-1 β release, s-GO (1–25 $\mu\text{g mL}^{-1}$, 22 h) was applied to murine immortalized bone-marrow-derived macrophages (iBMDMs) prior to addition of LPS (1 $\mu\text{g mL}^{-1}$, 2 h) and then ATP (5 mM, 1 h) ([Figure 1A](#)). s-GO alone did not induce cytotoxicity at any of the concentrations tested nor when followed by the addition of LPS to the culture medium ([Figure 1B](#)). This is important as we can now exclude cell death as an explanation for effects

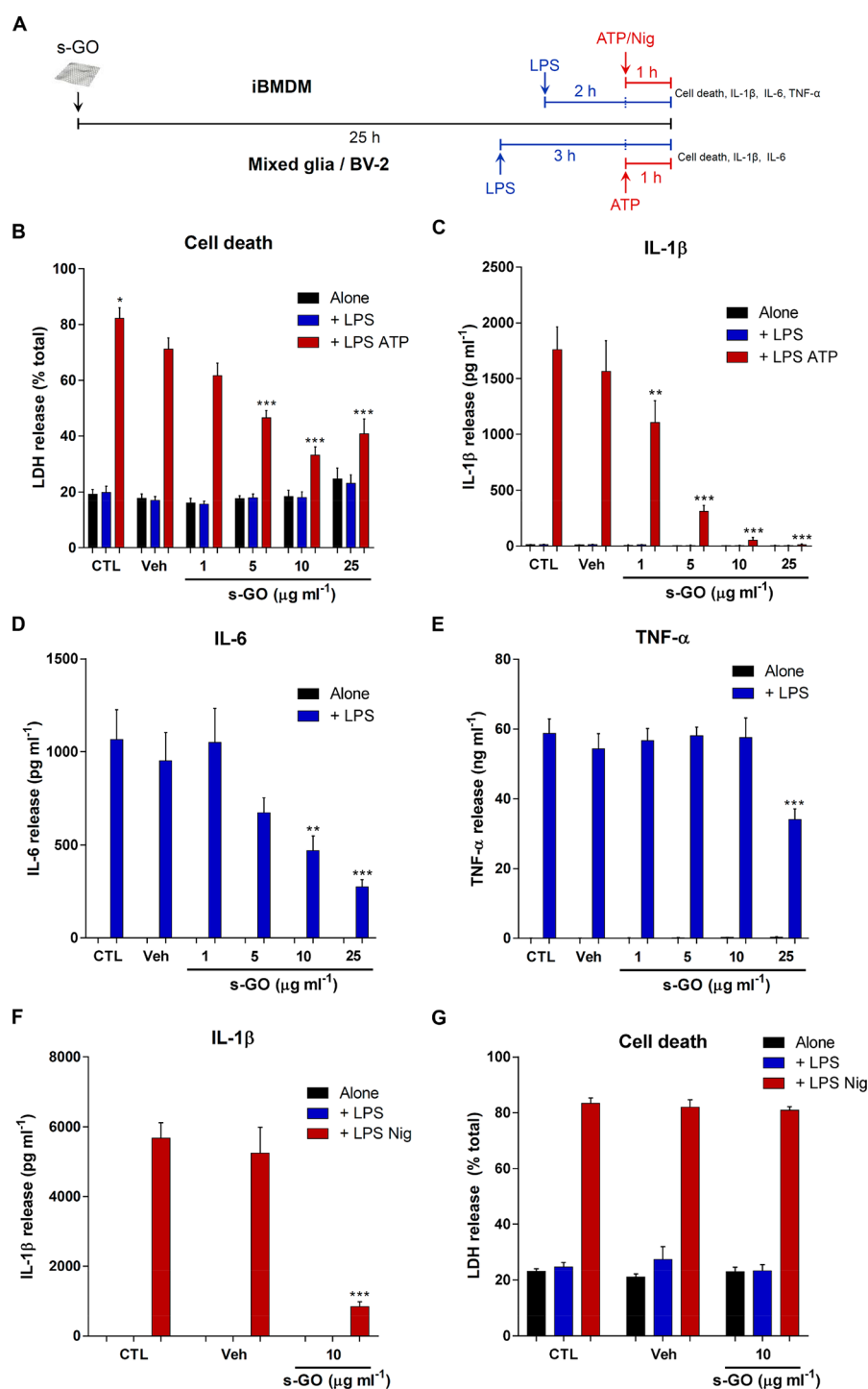


Figure 1. s-GO inhibits NLRP3 inflammasome-dependent IL-1 β release from iBMDMs. (A) Schematic of the cell treatment protocol. (B–E) iBMDMs were incubated in culture medium only, vehicle, or varying doses of s-GO (1–25 $\mu\text{g mL}^{-1}$, 22 h) before LPS (1 $\mu\text{g mL}^{-1}$, 2 h) was added directly to the culture medium, followed by ATP (5 mM, 1 h; $n = 4$). (B) Cell death, (C) IL-1 β release, (D) IL-6 release, and (E) TNF- α release were measured. (F,G) iBMDMs were incubated in culture medium only, vehicle, or s-GO (10 $\mu\text{g mL}^{-1}$, 22 h) before addition of LPS (1 $\mu\text{g mL}^{-1}$, 2 h) and nigericin (10 μM , 1 h; $n = 4$). (F) IL-1 β release and (G) cell death were measured. Cell death was measured as lactate dehydrogenase (LDH) release normalized to a total cell lysis control, and all cytokine measurements were carried out by ELISA. Data are presented as mean \pm SEM. Cytokine release and cell death assays were analyzed using two-way ANOVA with Dunnett's *posthoc* test (*versus* vehicle within each group). * $P < 0.05$; ** $P < 0.01$; *** $P < 0.001$.

observed on cytokine production. s-GO alone at any dose did not induce any IL-1 β , IL-6, or tumor necrosis factor (TNF)- α release compared with vehicle treatment, indicating that s-GO is not inherently pro-inflammatory (Figure 1C–E). Upon activation of the NLRP3 inflammasome with ATP, pretreat-

ment with s-GO reduced ATP-dependent cell death at doses of 5, 10, and 25 $\mu\text{g mL}^{-1}$, with the largest reduction observed at 10 $\mu\text{g mL}^{-1}$ (Figure 1B). s-GO treatment dose-dependently inhibited IL-1 β release from iBMDMs after inflammasome activation with LPS and ATP in comparison with vehicle-

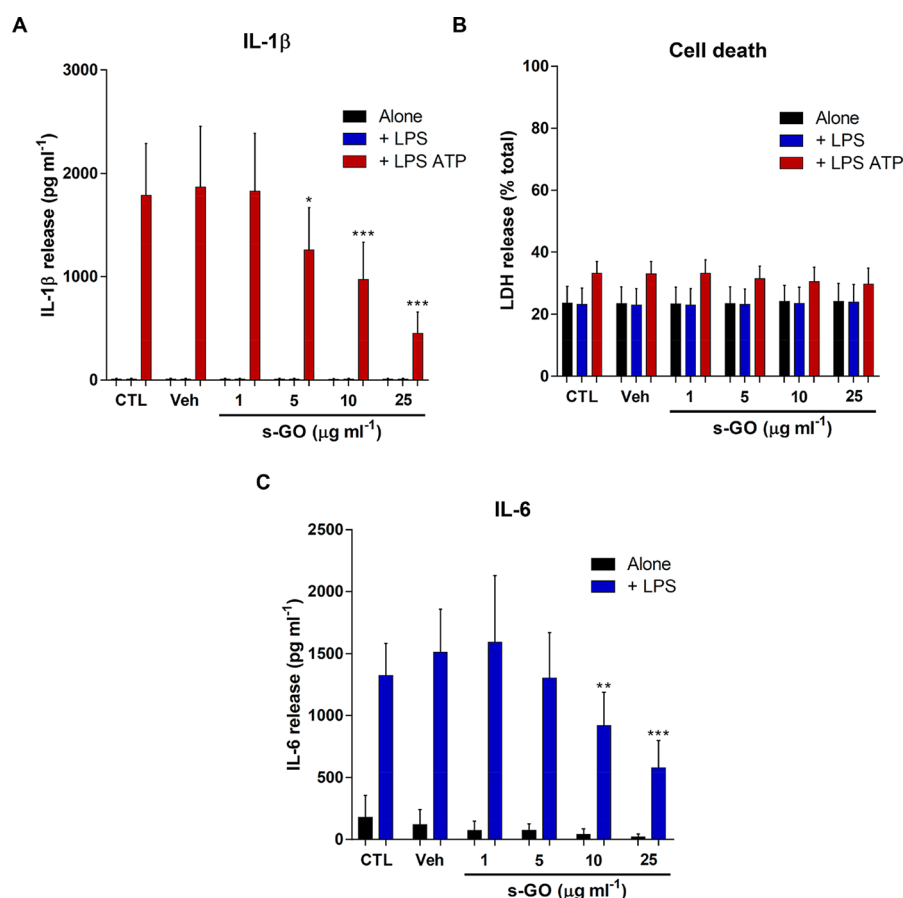


Figure 2. s-GO inhibits NLRP3 inflammasome-dependent IL-1 β release from mixed glia. (A–C) Mixed glial cells were incubated in culture medium only, vehicle, or varying doses of s-GO (1–25 $\mu\text{g mL}^{-1}$, 21 h) before LPS (1 $\mu\text{g mL}^{-1}$, 3 h) was added to the culture medium, followed by ATP (5 mM, 1 h; $n = 3$). (A) IL-1 β release, (B) cell death, and (C) IL-6 release were measured. Cell death was measured as LDH release normalized to a total cell lysis control, and all cytokine measurements were carried out by ELISA. Data are presented as mean \pm SEM. Data were analyzed using repeated measures two-way ANOVA with Dunnett's *posthoc* test (versus vehicle within each group). * $P < 0.05$; ** $P < 0.01$; *** $P < 0.001$.

treated cells (Figure 1C). LPS-induced IL-6 release was also significantly decreased by s-GO at 10 and 25 $\mu\text{g mL}^{-1}$, whereas TNF- α release was not significantly affected by s-GO apart from at 25 $\mu\text{g mL}^{-1}$ (Figure 1D,E). Furthermore, treatment with s-GO (10 $\mu\text{g mL}^{-1}$) prior to stimulation with nigericin, a P2X7 receptor-independent activator of NLRP3, also significantly inhibited IL-1 β release, indicating that the inhibitory effects of s-GO were not P2X7 receptor-dependent (Figure 1F). s-GO did not inhibit nigericin-induced cell death (Figure 1G). To further explore a potential structure–activity relationship between GO and IL-1 β release, we compared the effects of us- and l-GO sheets (Table 1 and Figure S2). The different sizes of GO (all 10 $\mu\text{g mL}^{-1}$) were added to iBMDMs for 22 h before the addition of LPS (1 $\mu\text{g mL}^{-1}$, 2 h) followed by nigericin (10 μM , 1 h). The effects of us-GO and l-GO on the expression and release of IL-1 β and release of IL-6 were comparable to the effects of s-GO, with the greatest effect observed with l-GO (Figure S2A–D).

Primary murine mixed glial cultures, which consist of astrocytes, microglia, and oligodendrocyte/type-2 astrocyte progenitor cells,³⁸ were treated with s-GO to assess whether these effects could be observed in brain-derived cells, indicating potential applications of s-GO in the brain. s-GO inhibition of interleukin release was not limited to iBMDMs, as s-GO also blocked LPS and ATP-induced IL-1 β release and

LPS-induced IL-6 release from mixed glial cells (Figure 2A,C). s-GO did not induce cell death either alone or when followed by LPS treatment (Figure 2B). s-GO did not affect ATP-induced cell death of the mixed glial cells (Figure 2B). To confirm that GO can influence microglial cell production of IL-1 β , we assessed GO's effect in mouse BV-2 microglia. BV-2 cells were treated with s-GO or l-GO (10 $\mu\text{g mL}^{-1}$, 21 h) and then treated with LPS (1 $\mu\text{g mL}^{-1}$, 3 h). Western blot of cell lysates showed that, consistent with the data in primary mixed glial cultures, in response to LPS, there was reduced IL-1 β in BV-2 microglia that had been treated with GO (Figure S3).

NLRP3 Inflammasome Activation Is Not Affected by s-GO, but Intracellular Expression of Pro-IL-1 β Is Reduced. Inflammasome activation is typified by the formation of an ASC speck, which results from the oligomerization of cytosolic ASC to act as a platform for caspase-1 recruitment.³² iBMDMs stably expressing ASC–mCherry³⁹ were pretreated with s-GO (10 $\mu\text{g mL}^{-1}$, 22 h) prior to LPS and nigericin stimulation (Figure 3A,Bi–v). Representative images of each treatment in the absence and presence of MCC950, a potent NLRP3 inflammasome inhibitor,⁴⁰ at a 2.75 h time point are shown (Figure 3A). s-GO alone did not induce ASC speck formation (Figure 3Bi). LPS alone induced some speck formation, and this was slightly reduced by s-GO treatment compared with vehicle treatment

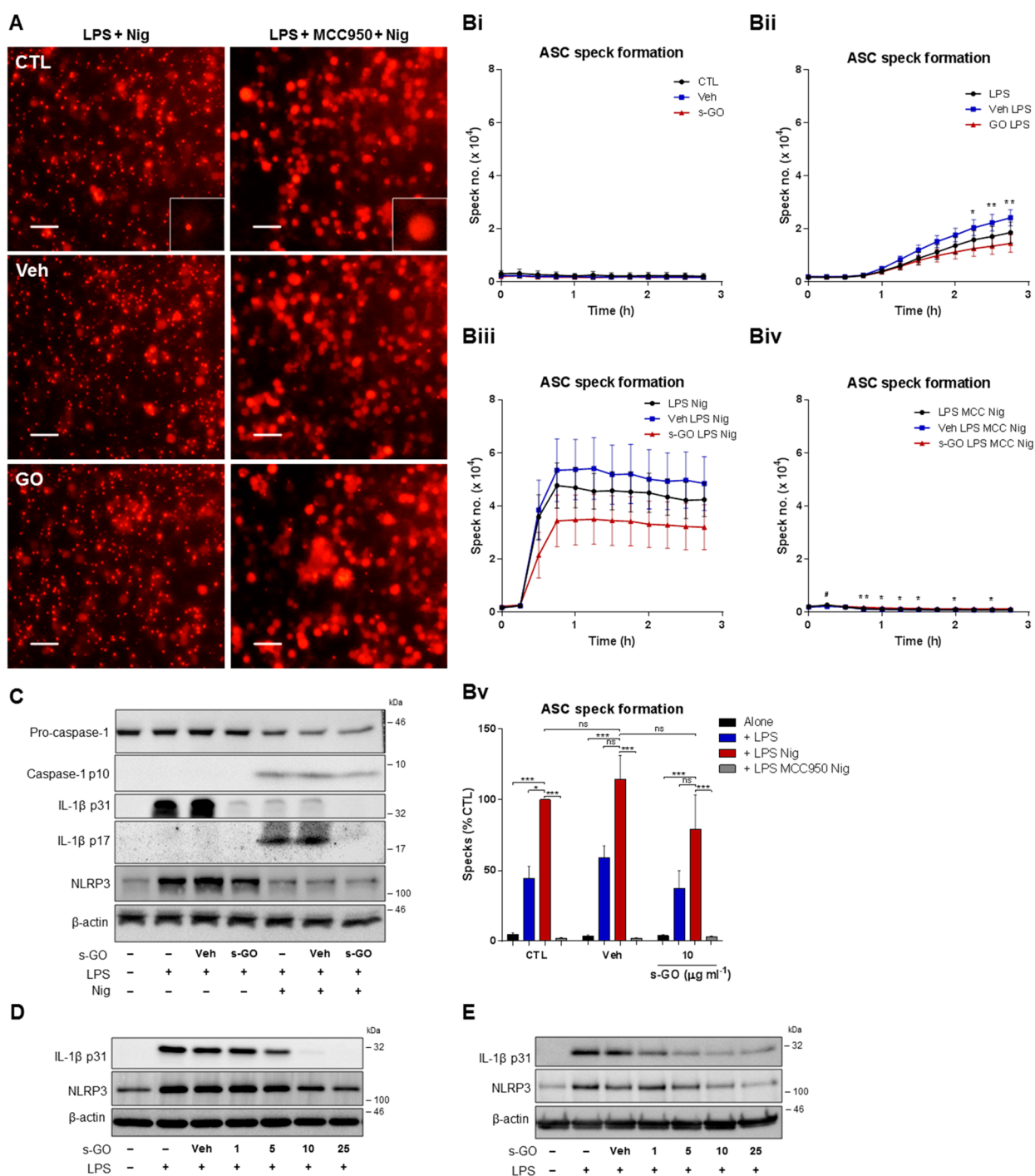


Figure 3. s-GO does not block ASC speck formation or caspase-1 maturation but depletes cytosolic pro-IL-1 β . (A,Bi–iv) iBMDMs stably expressing ASC–mCherry were incubated in culture medium alone, vehicle, or s-GO ($10 \mu\text{g mL}^{-1}$, 22 h) prior to stimulation with LPS ($1 \mu\text{g mL}^{-1}$, 2 h) and nigericin ($10 \mu\text{M}$, 2.5 h; $n = 4$). Speck formation was measured over a period of 2.75 h. A baseline image was acquired before addition of nigericin at 15 min. (A) Representative images from each group are shown in the absence and presence of MCC950 ($10 \mu\text{M}$). The scale bar represents $50 \mu\text{m}$. Insets in the control treatment images show an ASC speck in an activated cell or diffuse ASC in a cell treated with MCC950. ASC speck formation was measured over 2.75 h following (Bi) treatments alone, (Bii) treatments followed by LPS stimulation, (Biii) treatments followed by LPS and nigericin stimulation, or (Biv) in the presence of MCC950. (Bv) Number of ASC specks was assessed at 2.75 h. Speck formation was normalized to the LPS Nig control (no vehicle or s-GO pretreatment). (C) iBMDMs were incubated in culture medium alone, vehicle, or s-GO ($10 \mu\text{g mL}^{-1}$, 22 h) prior to stimulation with LPS ($1 \mu\text{g mL}^{-1}$, 2 h) and nigericin ($10 \mu\text{M}$, 1 h). Cells were lysed in-well and probed for caspase-1, IL-1 β , and NLRP3 by western blotting. (D) iBMDMs or (E) mixed glia were incubated in culture medium alone, vehicle, or s-GO (1 – $25 \mu\text{g mL}^{-1}$, 22 or 21 h) prior to stimulation with LPS ($1 \mu\text{g mL}^{-1}$, 2 or 3 h). Cell lysates were probed for IL-1 β and NLRP3 by western blotting. Data are presented as mean \pm SEM. Time course data were analyzed using two-way ANOVA with Dunnett's *posthoc* test. $\#P < 0.05$ CTL vs Veh; $*P < 0.05$ s-GO vs Veh; $***P < 0.01$ s-GO vs Veh. End time point data were analyzed using unmatched one-way ANOVA with Sidak's *posthoc* test; ns, not significant; $*P < 0.05$; $**P < 0.01$; $***P < 0.001$.

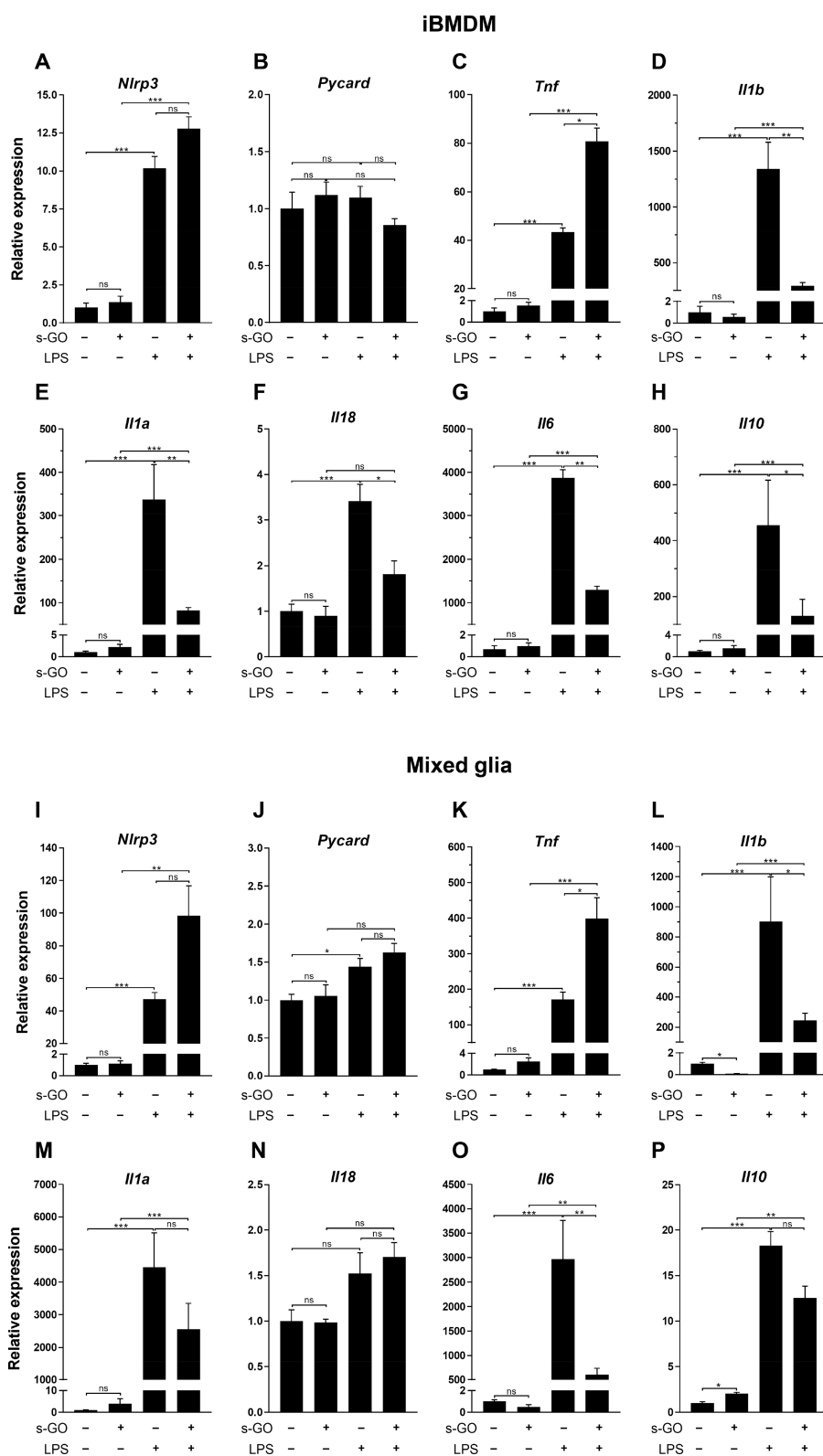


Figure 4. s-GO selectively inhibits LPS-induced interleukin mRNA expression. (A–H) iBMDMs were treated with vehicle or s-GO ($10 \mu\text{g mL}^{-1}$, 22 h) before the addition of LPS ($1 \mu\text{g mL}^{-1}$, 2 h; $n = 3$). (I–P) Mixed glia were treated with vehicle or s-GO ($25 \mu\text{g mL}^{-1}$, 21 h) before the addition of LPS (3 h; $n = 4$). The expression of various key inflammatory genes was assessed using RT-qPCR. Data are presented as mean \pm SEM and expressed relative to expression of a housekeeping gene and then normalized to the vehicle treatment. Data were analyzed using unmatched (iBMDM) or repeated measures (mixed glia) one-way ANOVA with Sidak's *posthoc* test; ns, not significant; * $P < 0.05$; ** $P < 0.01$; *** $P < 0.001$.

at the final three time points (Figure 3Bii). Specks formed 15–30 min after addition of nigericin in each treatment group and

peaked at approximately 1 h (Figure 3Biii). s-GO pretreatment did not inhibit ASC speck formation, whereas MCC950

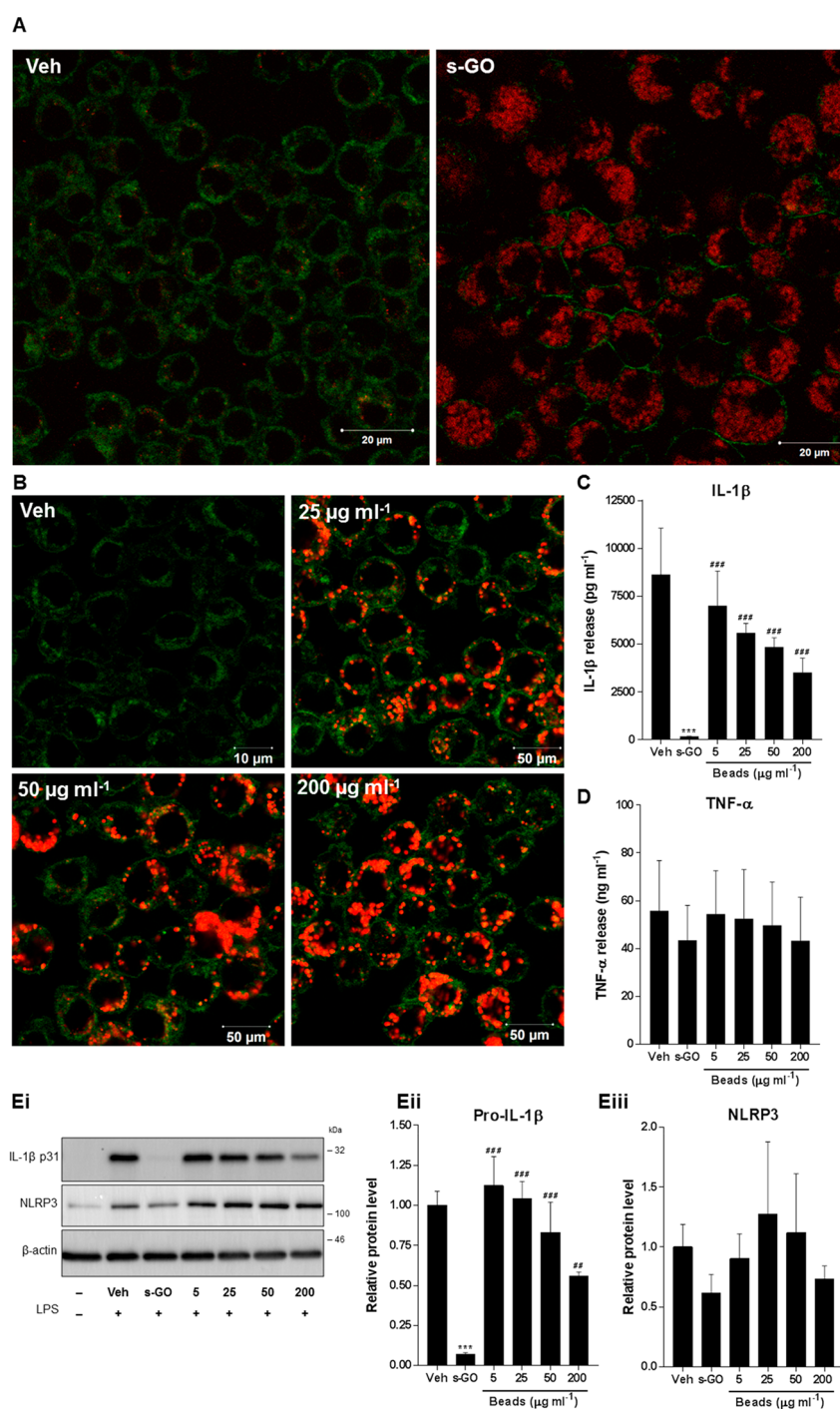


Figure 5. s-GO is efficiently internalized by macrophages. iBMDMs were treated with vehicle, s-GO ($25 \mu\text{g mL}^{-1}$), or red fluorescent carboxylate 100 nm diameter beads ($5, 25, 50, 200 \mu\text{g mL}^{-1}$, 22 h; $n = 3$). Uptake of (A) s-GO (594/620–690 nm, red) and (B) beads (580/605 nm, green) was imaged using a confocal microscope. Cell membranes were stained with CellMask Green plasma membrane stain (488/520 nm, green). Scale bars represent 10, 20, or 50 μm . (C–E) iBMDMs pretreated with s-GO or beads were stimulated with LPS ($1 \mu\text{g mL}^{-1}$, 2 h) and nigericin ($10 \mu\text{M}$, 1 h). Supernatants were analyzed by ELISA for (C) IL-1 β release upon LPS and ATP stimulation and (D) TNF- α release upon LPS priming. (Ei) Cell lysates of LPS-primed cells were probed for pro-IL-1 β and NLRP3 by western blotting. (Eii,iii) Densitometry for the pro-IL-1 β and NLRP3 western blots was performed on three independent experiments. Data are presented as mean \pm SEM. Data were analyzed using unmatched one-way ANOVA with Sidak's *posthoc* test. *** $P < 0.001$ versus vehicle-treated cells; ## $P < 0.01$; ### $P < 0.001$ versus GO-treated cells.

completely abolished ASC speck formation in response to nigericin treatment in all groups (Figure 3A,B,iii–v). Using western blotting, the active p10 caspase-1 fragment was observed in iBMDMs that had been treated with s-GO ($10 \mu\text{g mL}^{-1}$) followed by treatment with LPS and nigericin,

although this dose of s-GO inhibited IL-1 β release (Figure 3C). Western blotting was also used to show that the level of NLRP3 protein was not affected by s-GO treatment (Figure 3C). Together, these data suggested that s-GO inhibited IL-1 β release independently of NLRP3 inflammasome inhibition.

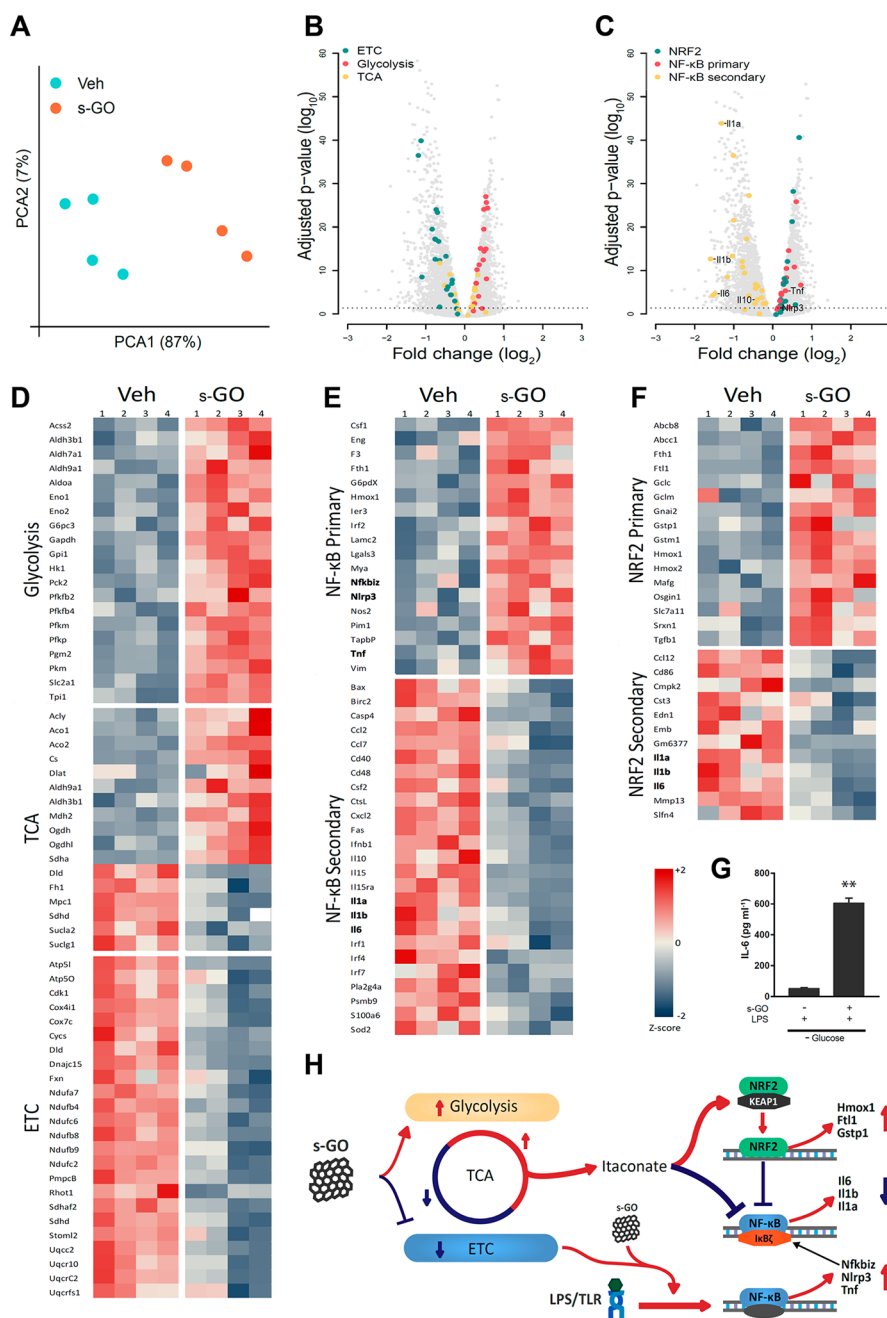


Figure 6. Transcriptomics demonstrate that s-GO causes a metabolomic shift which drives an anti-inflammatory response via NRF2 activation. iBMDMs were treated with vehicle or s-GO ($10 \mu\text{g mL}^{-1}$, 22 h) followed by LPS ($1 \mu\text{g mL}^{-1}$, 2 h). RNA-Seq was then performed. (A) Unguided principal component analysis revealed substantially different transcriptomic profiles between vehicle- and s-GO-treated cells. (B,C) Volcano plots showing a large number of genes both upregulated and downregulated by s-GO treatment, particularly highlighting the expression changes in genes involved in (B) glycolysis, the TCA cycle, and the ETC and (C) NF- κ B- and NRF2-regulated genes. (D) Heat maps of genes involved in glycolysis, the TCA cycle, and the ETC demonstrate a substantial shift to glycolysis and a shunt in the TCA cycle toward itaconate production. (E) Heat maps showing dichotomic NF- κ B responses to s-GO that correlate with $\kappa\text{B}\zeta$ dependence and NRF2 activation, both of which are modulated by itaconate. (F) Heat maps of NRF2-regulated genes, suggesting that s-GO causes NRF2 activation, and this mediates an anti-inflammatory response. (G) Anti-inflammatory effect of s-GO pretreatment ($10 \mu\text{g mL}^{-1}$, 22 h) on iBMDMs primed with LPS ($1 \mu\text{g mL}^{-1}$, 2 h) is abated and reversed when performed in glucose-free media (PBS, 2 mM CaCl₂, 10% FBS; $n = 2$), demonstrating the dependence of the anti-inflammatory effects of s-GO on metabolism. Data are presented as mean \pm SEM. Data were analyzed using a two-tailed unpaired t test. $**P < 0.01$. (H) Proposed mechanism of action of s-GO on metabolism and gene regulation.

Using western blotting, levels of pro-IL-1 β in the cell lysate were found to be much lower in cells that received s-GO treatment followed by LPS priming compared with cells treated with LPS in the absence of s-GO (Figure 3C). This was investigated further by assessing the level of cytosolic pro-IL-

1 β in response to TLR4 activation following treatment with varying doses of s-GO. There were dose-dependent decreases in LPS-induced pro-IL-1 β expression by s-GO treatment, with a much less pronounced decrease in NLRP3 protein levels only apparent at the higher s-GO doses (Figure 3D). Similar

decreases in cytosolic pro-IL-1 β were observed in mixed glial cells upon s-GO treatment (Figure 3E). Decreases in NLRP3 expression were also present at the higher doses of s-GO in the mixed glia (Figure 3E). s-GO did not limit LPS priming through sequestering LPS in the culture medium (Figure S4).

s-GO Inhibits Expression of *Il1b* mRNA. The selective inhibition of pro-IL-1 β expression prompted further investigation into the expression of inflammatory genes. iBMDMs were treated with s-GO (10 $\mu\text{g mL}^{-1}$, 22 h) and then primed with LPS (1 $\mu\text{g mL}^{-1}$, 2 h) prior to RT-qPCR analysis of genes involved in NLRP3 inflammasome activation or TLR4 signaling (Figure 4A–H). s-GO alone did not induce changes in levels of mRNA for *Nlrp3*, *Tnf*, *Il1b*, *Il1a*, *Il18*, *Il6*, or *Il10* (Figure 4A,C–H). As expected, LPS caused a large transcriptional upregulation of each of these inflammatory genes (Figure 4A,C–H). Consistent with s-GO's lack of effect on NLRP3 inflammasome formation, s-GO did not block LPS-induced upregulation of *Nlrp3* mRNA nor did s-GO affect expression of *Pycard* (ASC), which is constitutively expressed in macrophages (Figure 4A,B).²⁴ *Tnf* mRNA levels were increased by s-GO following LPS priming (Figure 4C). However, s-GO treatment significantly attenuated LPS-induced increases in the mRNA of *Il1b*, *Il1a*, *Il18*, *Il6*, and *Il10* (Figure 4D–H).

Similar observations were made in mixed glial cells that were treated with s-GO (25 $\mu\text{g mL}^{-1}$, 21 h) before priming with LPS (1 $\mu\text{g mL}^{-1}$, 3 h; Figure 4I–P). Following priming, s-GO did not significantly affect the upregulation of *Nlrp3* or *Il10* mRNA, and *Tnf* expression was again increased (Figure 4I,K,P). Although *Pycard* (ASC) was upregulated by LPS priming in the vehicle group, no differences were observed between s-GO and vehicle treatments (Figure 4J). *Il18* expression was not significantly induced by LPS and was not affected by s-GO (Figure 4N). s-GO significantly blocked LPS-induced increases in *Il1b* and *Il6* mRNA, although no significant inhibition of *Il1a* mRNA was detected in response to s-GO pretreatment (Figure 4L,M,O). s-GO alone, in the absence of LPS, caused a reduction in expression of *Il1b* and an increase in the expression of *Il10* compared with vehicle treatment alone but did not cause significant changes in the other inflammatory genes assessed (Figure 4L,P).

s-GO Is Efficiently Internalized Prior to LPS Priming.

The cellular uptake of s-GO (25 $\mu\text{g mL}^{-1}$, 22 h) was assessed in iBMDMs by exploiting the autofluorescent properties of s-GO using live cell confocal microscopy.⁴¹ s-GO was readily taken up into cells and localized in phagolysosomal compartments, occupying a large proportion of the cytoplasm (Figure 5A). To assess whether the process of particle phagocytosis *per se* was responsible for the inhibition of pro-IL-1 β expression, the uptake of red fluorescent (580/605 nm) beads (5, 25, 50, 200 $\mu\text{g mL}^{-1}$, FluoSpheres carboxylate-modified microspheres, Invitrogen) was assessed. In order to mimic the lateral dimensions and surface charge of s-GO, carboxyl-functionalized beads with a diameter of 100 nm were chosen. These beads were also found to be taken up efficiently by iBMDMs, localizing in morphologically similar compartments as s-GO (Figure 5B). Upon priming and subsequent activation of the inflammasome, the 100 nm carboxylate beads did not inhibit IL-1 β release at any of the doses tested in comparison with vehicle, whereas s-GO (25 $\mu\text{g mL}^{-1}$) did inhibit IL-1 β release in comparison with both vehicle and each bead concentration (Figure 5C). TNF- α release from LPS-primed cells was not affected by pretreatment with s-GO or the fluorescent

carboxylate beads (Figure 5D). Furthermore, the carboxylate beads did not significantly decrease the amount of pro-IL-1 β in the cell lysate, whereas s-GO reduced pro-IL-1 β protein in comparison with both vehicle and each bead concentration (Figure 5E_{i,ii}). No significant effect was seen on NLRP3 protein levels in any of the treatment groups (Figure 5E_{i,iii}). These data, and the data presented in Figure S2, suggest that s-GO-dependent inhibition of interleukin expression is not simply due to the process of particle phagocytosis.

Elucidating the Mechanism of s-GO-Dependent Inflammatory Gene Regulation.

To establish the mechanism of action of GO, we treated iBMDMs with vehicle or s-GO (10 $\mu\text{g mL}^{-1}$, 22 h) prior to priming with LPS (1 $\mu\text{g mL}^{-1}$, 2 h) and then extracted the RNA for analysis by RNA-Seq. Unguided principal component analysis of the data revealed substantially different transcriptomic profiles between vehicle- and s-GO-treated cells (Figure 6A). Consistent with the data presented in Figures 1–4, s-GO caused the selective inhibition of certain inflammatory genes (*e.g.*, *Il6*, *Il1b*, and *Il1a*), but overall, the NF- κ B pathway was not inhibited (Figure 6C,E). The division between these NF- κ B responses correlated with a recently identified regulatory mechanism of NF- κ B gene regulation involving the transcription factor I κ B ζ , which is necessary for expression of *Il6*, *Il1b*, and *Il1a*.⁴² To elucidate the potential mechanism of I κ B ζ -NF- κ B inhibition, enrichment analyses were performed on the RNA-Seq data set. From this, it was observed that a clear shift in immunometabolism had occurred in the s-GO-treated cells. Glycolysis-associated genes were substantially upregulated, electron transport chain (ETC) genes were downregulated, and the tricarboxylic acid (TCA) cycle genes were dichotomically modulated (Figure 6B,D). This metabolic shift would result in substantial changes to the metabolome of the cells, including a pivot in the TCA cycle, leading to accumulation of the metabolite itaconate. Itaconate was recently discovered to have substantial anti-inflammatory effects which target I κ B ζ -regulated genes, including *Il6* and *Il1b*, without altering NF- κ B primary genes such as *Tnf* (Figure 6H).^{42,43} To further study the importance of glycolysis–TCA metabolism for the anti-inflammatory effects of GO, an additional iBMDM experiment was performed in the absence of the primary metabolic substrate glucose. iBMDMs were treated with vehicle or s-GO (10 $\mu\text{g mL}^{-1}$, 22 h) in phosphate-buffered saline (PBS) containing 2 mM CaCl₂ and 10% fetal bovine serum (FBS) prior to LPS priming (1 $\mu\text{g mL}^{-1}$, 2 h). We found that without input into glycolysis–TCA metabolism, the anti-inflammatory effects of s-GO were completely abated, and an underlying pro-inflammatory effect of s-GO was revealed (Figure 6G). This provided further evidence that s-GO was anti-inflammatory through alterations in glycolysis–TCA metabolism, potentially involving the metabolite itaconate.

The previously identified mechanism of itaconate-induced I κ B ζ inhibition is both a direct effect of itaconate on I κ B ζ -NF- κ B transcription, as well as itaconate inducing the activation of the transcription factor nuclear factor erythroid 2-related factor 2 (NRF2). Thus, if itaconate was the central mediator of the anti-inflammatory effect of GO, NRF2-regulated genes should be upregulated in the RNA-Seq data set, and indeed, this is exactly what was observed. Further RNA-Seq enrichment analyses were performed, and a substantial enrichment of NRF2-regulated genes was found, with upregulation of *Hmox1*, *Ftl1*, and *Gstp1* (Figure 6F) and downregulation of genes previously identified to be negatively

regulated by NRF2 *via* the inhibition of RNA Pol II recruitment to I κ B ζ -NF- κ B-regulated genes, including *Il1b*, *Il1a*, and *Il6*.⁴⁴ Thus, we propose that GO treatment causes a profound effect on cellular metabolism, resulting in the activation of the anti-inflammatory transcription factor NRF2, which both upregulates anti-inflammatory genes and downregulates I κ B ζ -NF- κ B-regulated pro-inflammatory genes, including *Il1b* and *Il6*.

DISCUSSION

GO sheets have shown promise in various biomedical applications, including tissue engineering and drug delivery; however, their interactions with the innate immune system, and specifically inflammasomes, remain poorly defined.^{3,6} This study aimed to determine the effects of s-GO on inflammasome responses in macrophage cells. To the best of our knowledge, no previous studies have assessed the impact of s-GO pretreatment on inflammasome priming after subsequent TLR4 stimulation. Importantly, we report that, in the absence of LPS, s-GO applied alone up to a concentration of 25 μ g mL⁻¹ for 24 hours was neither toxic nor pro-inflammatory and did not activate the inflammasome. However, we report marked inhibition of NLRP3-dependent IL-1 β release following s-GO pretreatment due to a reduction in the levels of pro-IL-1 β . These findings were independent of effects on NLRP3 expression and inflammasome activation, as ASC speck formation and caspase-1 activation were unaffected. Instead, we provide evidence for the selective inhibition of interleukin gene expression by s-GO, revealing dissociation in the mechanisms regulating genes downstream of TLR4 signaling. This effect is very likely due to the effects of s-GO on cellular metabolism and the activation of the anti-inflammatory transcription factor NRF2, which is known to inhibit IL-1 β and IL-6 expression (but not TNF- α).⁴²⁻⁴⁴ These data show that s-GO can be used as a tool to dissect and highlight inflammatory mechanisms, and that treating cells with s-GO has profound and complex responses. The anti-inflammatory effects of GO may have important implications for clinical applications, although further research is required. These findings are supported by Chen *et al.*, who also suggest an anti-inflammatory effect of GO in microglial cells.⁴⁵ Furthermore, GO is reported to profoundly affect the physiology of astrocytes in culture.⁴⁶

Several studies have demonstrated that s-GO is readily taken up by macrophages.⁴⁷⁻⁴⁹ Previous studies have also investigated the potential inflammatory effects of GO in macrophages. Ma *et al.* showed that l-GO elicited stronger NF- κ B activation and pro-inflammatory cytokine expression than s-GO both *in vitro* and *in vivo*.⁴⁷ However, the lateral size of GO may exert contrasting effects on pro-inflammatory cytokine expression in human immune cells, as s-GO induces stronger expression of cytokines in human peripheral blood mononuclear cells than l-GO.⁵⁰ However, in this study, we find that the effects of us-GO, s-GO, and l-GO are comparable with respect to IL-1 β and IL-6 production (Figure S2). Higher concentrations of GO also appear to induce NF- κ B signaling *via* TLR4 in RAW264.7 cells and can induce IL-1 β release from LPS-primed THP-1 macrophages.^{51,52} A recent study by Mukherjee *et al.*, in contrast to our findings, demonstrated that 50 μ g mL⁻¹ of s-GO, which is double that of the highest dose used in this study, was able to induce IL-1 β release from human monocyte-derived macrophages and THP-1 cells that had already been primed with LPS, and that this was abolished

in NLRP3-deficient cells.⁵³ The differences between these studies, in terms of the dose of s-GO used as well as the timing of treatment relative to LPS priming, may be sufficient to explain these contrasting results. Our findings add further evidence to the notion that GO is able to influence the inflammatory response of macrophage cells, in this case by GO pretreatment blocking the LPS-induced expression of inflammatory genes through a shift in immunometabolism.

Key considerations must be taken into account when evaluating studies investigating the inflammatory effects of GO. Having serum in the culture medium improves the dispersion of GO due to adsorption of serum proteins, limiting GO aggregation.⁴¹ Particulates such as silica and monosodium urate crystals are well characterized as NLRP3 inflammasome activators.^{29,54,55} Thus, in the absence of serum, the altered physicochemical properties of GO may modify the resulting inflammatory response. Hence, serum was maintained in the culture medium throughout this study. Recent evidence also indicates that endotoxin contamination of GO solutions can alter the response of cells to GO, as well as inducing pro-inflammatory effects alone.³⁷ Therefore, endotoxin contamination must be considered as a potential confounding factor when assessing the pro-inflammatory effects of GO. Although not directly relevant to this study, we nonetheless found no evidence of endotoxin contamination in our s-GO, prior to direct stimulation of the cells with LPS itself.

Further work is required to fully characterize the effects of GO on macrophages and microglia. It is becoming increasingly apparent that GO exerts a multitude of biological effects,⁵⁶ and we report here a profound effect on gene expression profile with a major impact on metabolism. These effects of s-GO are likely due to an activation of NRF2 caused by the metabolic reprogramming of the cell, rather than a direct effect on the TLR4-NF- κ B pathway. NRF2 then exerts its anti-inflammatory effects through the downregulation of genes such as *Il1b* and *Il6*.

CONCLUSIONS

GO holds promise for use in biological applications. To facilitate this, a greater understanding of how GO interacts with macrophage cells is required. We have shown that GO alone has no overt pro-inflammatory effect on macrophage cells. In fact, we found an inhibitory effect of GO on cytokine production in macrophages, specifically by inhibiting interleukin expression upon TLR4 stimulation, without inhibiting subsequent activation of the inflammasome. We propose that this inhibitory effect is due to an activation of NRF2 caused by the metabolic reprogramming of the cell in response to GO. These data provide insights into the effects of GO and highlight GO as a potential tool to elucidate a better mechanistic understanding of underlying inflammatory pathways.

METHODS

Synthesis and Characterization of GO Sheets. We used graphite flakes (Graflake 9580, Nacional Grafite Ltd., Brazil) to produce GO. We used the modified Hummers method described previously to synthesize GO sheets.^{57,58} Synthesis and full physicochemical characterization of the thin GO sheets with distinct lateral dimensions used in this study (*i.e.*, l-, s-, and us-GO) has already been reported.³⁶

A multimode AFM was used to characterize the GO. It was used on the tapping mode with a J-type scanner, a Nanoscope V8 controller

(Veeco, Cambridge, UK), and an OTESPA silicon probe (Bruker, UK). Twenty microliters of 100 $\mu\text{L mL}^{-1}$ of GO was deposited on a freshly cleaved mica surface (Agar Scientific, Essex, UK) coated with 0.01% poly-L-lysine (Sigma-Aldrich, UK) and was allowed to adsorb for 5 min before images were taken in air.

Cell Culture. *Immortalized Bone-Marrow-Derived Macrophages.* iBMDMs were a gift from Professor Clare Bryant (Department of Veterinary Medicine, University of Cambridge). Cells were cultured in Dulbecco's modified Eagle's medium (DMEM) containing 10% FBS (Life Technologies), 100 U mL^{-1} of penicillin, and 100 $\mu\text{g mL}^{-1}$ of streptomycin (PenStrep). Cells were seeded at 7.5×10^5 cells mL^{-1} , incubated overnight at 37 °C, 90% humidity, and 5% CO_2 in 24-well plates, and treated the following day.

Primary Murine Mixed Glia. Murine mixed glia cells were prepared from the brains of 2–4-day-old C57BL/6 mice. Briefly, the cerebral hemispheres were dissected and the meninges were then removed. The remaining tissue was homogenized in DMEM containing 10% FBS and PenStrep *via* repeated trituration. The resulting homogenate was centrifuged at 800g for 10 min, and the pellet was resuspended in fresh culture medium before being incubated in a flask at 37 °C, 90% humidity, and 5% CO_2 . After 5 days, the cells were washed, and fresh medium was placed on the cells. The medium was replaced every 2 days. On day 12, the cells were seeded at 2×10^5 cells mL^{-1} in 24-well plates and incubated for a further 2 days prior to use.

Assays. Cells were either untreated or treated with vehicle (culture medium containing 1% H_2O) or GO (1, 5, 10, or 25 $\mu\text{g mL}^{-1}$) in culture medium containing 10% FBS for 22 h (iBMDMs) or 21 h (mixed glia), and LPS (1 $\mu\text{g mL}^{-1}$) was then added to the well for a further 2 h (iBMDMs) or 3 h (mixed glia). Inflammasome activation was induced by adding ATP (5 mM, Sigma) or nigericin (10 μM , Sigma) to the well for 1 h, and the supernatants were analyzed for IL-1 β , IL-6, and TNF- α content. iBMDMs were also treated with red fluorescent carboxylate 100 nm diameter beads (5, 25, 50, or 200 $\mu\text{g mL}^{-1}$, 22 h; FluoSpheres carboxylate-modified microspheres, Invitrogen) prior to LPS and nigericin stimulation. Lysates of cells that did not receive ATP or nigericin stimulation were assessed for pro-IL-1 β and NLRP3 expression. Cells that received inflammasome activation were probed for caspase-1 activation by western blotting. To investigate glucose-dependent functions of s-GO, iBMDMs were treated with vehicle or s-GO (10 $\mu\text{g mL}^{-1}$, 22 h) in PBS containing 10% FBS and 2 mM CaCl_2 . LPS (1 $\mu\text{g mL}^{-1}$) was then added to the well for a further 2 h. The supernatant was analyzed for IL-6 content.

Western Blotting. Cells were lysed with lysis buffer (50 mM Tris/HCl, 150 mM NaCl, Triton 1% v/v, pH 7.3) containing protease inhibitor cocktail (Calbiochem), centrifuged at 12 000g (15 min) at 4 °C and analyzed for IL-1 β , NLRP3, and caspase-1. Samples were run on sodium dodecyl sulfate–polyacrylamide gels and transferred at 25 V onto nitrocellulose or polyvinylidene fluoride membranes using a Trans-Blot Turbo transfer system (Bio-Rad). Membranes were blocked in either 5% w/v milk or 5% bovine serum albumin (BSA) in PBS, 0.1% Tween 20 (PBST) for 1 h at room temperature. The membranes were then washed with PBST and incubated at 4 °C overnight with goat anti-mouse IL-1 β (250 ng mL^{-1} ; R&D Systems), mouse anti-mouse NLRP3 (1 $\mu\text{g mL}^{-1}$; Adipogen), or rabbit anti-mouse caspase-1 (1.87 $\mu\text{g mL}^{-1}$; Abcam) primary antibodies in 0.1% (IL-1 β) or 1% (NLRP3) BSA or 5% milk (caspase-1) in PBST. Membranes were washed and incubated with rabbit anti-goat (500 ng mL^{-1} , 5% milk in PBST; Dako), rabbit anti-mouse (1.3 $\mu\text{g mL}^{-1}$, 1% BSA PBST; Dako), or goat anti-rabbit IgG (250 ng mL^{-1} , 5% milk in PBST; Dako) at room temperature for 1 h. Proteins were then visualized with Amersham ECL Western blotting detection reagent (GE Life Sciences) and G:BOX (Syngene) and Genesys software. β -Actin was used as a loading control. Densitometry was performed using ImageJ software.

Cell Death Assay. Cell death was assessed by measuring lactate dehydrogenase release using a CytoTox 96 nonradioactive cytotoxicity assay (Promega) according to the manufacturer's instructions. All supernatants were centrifuged at 12 000g (10 min) at 4 °C prior to analysis in order to remove GO from the supernatant, minimizing any potential effect on absorbance measurements.

ELISA. The levels of the cytokines IL-1 β , IL-6, and TNF- α in the supernatant were analyzed by enzyme-linked immunosorbent assay (ELISA; DuoSet, R&D systems) according to the manufacturer's instructions. All supernatants were centrifuged at 12 000g (10 min) at 4 °C prior to analysis in order to remove GO from the supernatant.

ASC Speck Imaging. iBMDMs stably expressing ASC–mCherry³⁹ were used to perform live imaging of ASC speck formation. Cells were seeded at 7.5×10^5 cells mL^{-1} in 96-well plates and incubated overnight. The following day, cells were treated with s-GO (10 $\mu\text{g mL}^{-1}$, 22 h) or vehicle in FluoroBrite DMEM (Thermo) containing 10% FBS and PenStrep, and LPS (1 $\mu\text{g mL}^{-1}$, 2 h) was then added to the wells to induce priming. All cells were then preincubated with the pan-caspase inhibitor Z-VAD-FMK (50 μM , 15 min; Sigma) to prevent pyroptotic cell death, prior to the addition of nigericin. During this preincubation, some cells were simultaneously treated with MCC950 (10 μM , 15 min; Sigma), a selective inhibitor of NLRP3 inflammasome activation and speck formation,⁴⁰ and a baseline image was acquired on an InCuCyte ZOOM live cell analysis system (Essen Bioscience) at 37 °C using a 20 \times /0.61 S Plan Fluor objective. Nigericin (10 μM) was then added to activate the NLRP3 inflammasome, and images were acquired every 15 min for a further 2.75 h. Speck number was quantified using InCuCyte ZOOM software and was assessed for each treatment at the final time point of 2.75 h.

RT-qPCR. s-GO was applied to iBMDMs (10 $\mu\text{g mL}^{-1}$, 22 h) and mixed glia (25 $\mu\text{g mL}^{-1}$, 21 h) before the addition of LPS (1 $\mu\text{g mL}^{-1}$, 2 or 3 h). RNA was extracted using a PureLink RNA mini kit (Invitrogen). Reverse transcription was performed from 1 μg of total RNA with M-MLV reverse transcriptase (Invitrogen). qPCR was performed using iQ SYBR Green Supermix (Bio-Rad) containing 200 nM of each primer. The primers designed for each gene are in Table S1. Assays were run using a 7900HT fast real-time PCR system (Applied Biosystems), with the following cycle conditions: 50 °C (2 min); 95 °C (10 min); 40 cycles of 95 °C (15 s) and 60 °C (1 min). Hydroxymethylbilane synthase (*Hmbs*) was used as the housekeeping gene. The levels of expression of each gene of interest were computed as follows: relative mRNA expression = $(E - (C_t \text{ of gene of interest})) / (E - (C_t \text{ of housekeeping gene}))$, where C_t is the threshold cycle value and E is efficiency.

RNA-Seq. iBMDMs were treated with vehicle or s-GO (10 $\mu\text{g mL}^{-1}$, 22 h) prior to priming with LPS (1 $\mu\text{g mL}^{-1}$, 2 h). RNA was extracted using a PureLink RNA mini kit (Invitrogen). RNA-Seq analysis was performed. RNA samples were assessed for quality and integrity using a 2200 TapeStation (Agilent Technologies) according to the manufacturer's instructions. RNA-Seq libraries were generated using the TruSeq Stranded mRNA assay (Illumina, Inc.) according to the manufacturer's instructions. Briefly, poly-T, oligo-attached, magnetic beads were used to extract polyadenylated mRNA from 1 μg of total RNA. The mRNA was then fragmented using divalent cations under high temperature and then transcribed into first strand cDNA using random primers. Second strand cDNA was then synthesized using DNA polymerase I and RNase H, and a single "A" base addition was performed. Adapters were then ligated to the cDNA fragments and then purified and enriched by PCR to create the final cDNA library. Adapter indices were used to multiplex libraries, which were pooled prior to cluster generation using a cBot instrument. The loaded flow cell was then pair-end sequenced (101 + 101 cycles, plus indices) on an Illumina HiSeq4000 instrument. Demultiplexing of the output data (allowing one mismatch) and BCL-to-Fastq conversion was performed with CASAVA 1.8.3. Sequencing quality for each sample was determined using the FastQC program. Low-quality sequence data were removed utilizing the trimmomatic program. STAR v2.4.0 was utilized to map the trimmed sequence into the murine genome (mm10 genome with gencode M16 annotation). Raw counts for each sample were generated by the htseq-count program and subsequently normalized relative to respective library sizes using DESeq2 package for the R statistical program.^{59,60} The DESeq2 program was additionally used to plot the PCA with all sample data to visualize different clusters at multiple levels that describes the maximum variance within the data set. Genes of interest

were identified by pairwise comparisons. False discovery rate (FDR) adjusted p values were used to evaluate significance.

Functional and Pathway Enrichment Analysis. Genes with an FDR-corrected p value of less than 0.01 were analyzed for transcriptional regulation, cell pathway, and cell localization enrichment utilizing the Enrichr gene set enrichment analysis web server.^{61,62} Significant features ($p < 0.05$) were then further investigated for consistency in response direction to identify the key mechanism involved in the s-GO response. From this, the transcription factor NRF2 ($p = 1.2 \times 10^{-15}$), cell pathways of glucose entry into the TCA cycle ($p = 0.0002$) and glycolysis ($p = 0.0037$), and the mitochondrial inner membrane cell compartment ($p = 5.8 \times 10^{-26}$) were identified. Gene lists found to be enriched in these features were then used to generate heat maps to visualize the effects of s-GO.

Confocal Microscopy. iBMDMs were plated out at 3.75×10^5 cells mL^{-1} overnight in a Cellview cell culture dish (627870; Greiner Bio-One Ltd.). The following day, cells were treated with vehicle, s-GO ($25 \mu\text{g mL}^{-1}$), or red fluorescent (580/605 nm) carboxyl-functionalized 100 nm diameter beads (5, 25, 50, or $200 \mu\text{g mL}^{-1}$, 22 h; FluoSpheres carboxylate-modified microspheres, Invitrogen). Cell membranes were then stained with CellMask Green plasma membrane stain (C37608, dilution 1:2500, 488/520 nm; Thermo Scientific), whereas s-GO exhibited autofluorescence (594/620–690 nm). Cells were viewed using a Zeiss 780 multiphoton confocal laser scanning microscope with a 40 \times objective. Images were subsequently processed using ZEN, the Zeiss microscope software.

Data Analysis. Data are presented as the mean \pm standard error of the mean (SEM). Data were analyzed using two-tailed unpaired t tests, unmatched and repeated measures one-way analysis of variance (ANOVA) with Sidak's *posthoc* test, or unmatched and repeated measures two-way ANOVA with Dunnett's *posthoc* test using GraphPad Prism (v7). RNA-Seq data were analyzed as above using DESeq2⁵⁹ on R version 3.5.1.⁶⁰ Transformations or corrections were applied as necessary to obtain equal variance between groups prior to analysis. Statistical significance was accepted at * $P < 0.05$, ** $P < 0.01$, and *** $P < 0.001$.

ASSOCIATED CONTENT

Supporting Information

The Supporting Information is available free of charge on the ACS Publications website at DOI: 10.1021/acsnano.8b03642. The RNA-Seq data set can be explored using this online tool: <https://braininflammationgroup-universityofmanchester.shinyapps.io/GrapheneOxide/>.

Primer sequences for the genes analyzed using RT-qPCR; Figures S1–S4 (PDF)

AUTHOR INFORMATION

Corresponding Author

*E-mail: david.brough@manchester.ac.uk. Tel: +44 (0)161 275 5039. Fax: +44 161 275 5948.

ORCID

Sandra Vranic: 0000-0002-6653-7156

Kostas Kostarelos: 0000-0002-2224-6672

David Brough: 0000-0002-2250-2381

Author Contributions

D.B., K.K., S.M.A., and N.J.R. and were responsible for conception of the project. C.H., J.R.-A., E.L., E.W., and D.B. designed and performed the experiments. S.V. and M.B. contributed to the characterization of s-GO. S.V. performed the uptake experiments using confocal microscopy. J.R.-A. analyzed the RNA-Seq data set. C.H. wrote the manuscript, with support from E.L., S.V., J.R.-A., K.K., S.M.A., N.J.R., and D.B. J.R.-A. and E.L. contributed equally to this work.

Notes

The authors declare no competing financial interest.

ACKNOWLEDGMENTS

This work was funded by the MRC (Grant No. MR/N003586/1 to D.B., K.K., S.M.A., and N.J.R.) and was also funded by an MRC PhD studentship to C.H. (Grant No. MR/N013751/1). J.R.-A. was funded by the BBSRC (BB/P01061X/1). This work was partially funded by the European Union's seventh RTD Framework Program: Graphene Flagship project (FP7-ICT-2013-FET-F-604391) and has received funding from the European Union's Horizon 2020 research and innovation programme under Grant Agreement No. 696656 (Graphene Flagship Core1).

REFERENCES

- (1) Novoselov, K.; Geim, A.; Morozov, S.; Jiang, D.; Zhang, Y.; Dubonos, S.; Grigorieva, I.; Firsov, A. Electric Field Effect in Atomically Thin Carbon Films. *Science* **2004**, *306*, 666–669.
- (2) Geim, A.; Novoselov, K. The Rise of Graphene. *Nat. Mater.* **2007**, *6*, 183–191.
- (3) Muthoosamy, K.; Bai, R.; Manickam, S. Graphene and Graphene Oxide as a Docking Station for Modern Drug Delivery System. *Curr. Drug Delivery* **2014**, *11*, 701–718.
- (4) Yoo, J. M.; Kang, J. H.; Hong, B. H. Graphene-Based Nanomaterials for Versatile Imaging Studies. *Chem. Soc. Rev.* **2015**, *44*, 4835–4852.
- (5) Wang, Z.; Dai, Z. Carbon Nanomaterial-Based Electrochemical Biosensors: An Overview. *Nanoscale* **2015**, *7*, 6420–6431.
- (6) Ding, X.; Liu, H.; Fan, Y. Graphene-Based Materials in Regenerative Medicine. *Adv. Healthcare Mater.* **2015**, *4*, 1451–1468.
- (7) Brough, D.; Rothwell, N. J.; Allan, S. M. Interleukin-1 as a Pharmacological Target in Acute Brain Injury. *Exp. Physiol.* **2015**, *100*, 1488–1494.
- (8) Heneka, M. T.; Kummer, M. P.; Stutz, A.; Delekate, A.; Schwartz, S.; Vieira-Saecker, A.; Griep, A.; Axt, D.; Remus, A.; Tzeng, T.; Gelpi, E.; Halle, A.; Korte, M.; Latz, E.; Golenbock, D. T. NLRP3 Is Activated in Alzheimer's Disease and Contributes to Pathology in APP/PS1 Mice. *Nature* **2012**, *493*, 674–678.
- (9) Denes, A.; Coutts, G.; Lénárt, N.; Cruickshank, S. M.; Pelegrin, P.; Skinner, J.; Rothwell, N.; Allan, S. M.; Brough, D. AIM2 and NLRP3 Inflammasomes Contribute with ASC to Acute Brain Injury Independently of NLRP3. *Proc. Natl. Acad. Sci. U. S. A.* **2015**, *112*, 4050–4055.
- (10) Coussens, L. M.; Werb, Z. Inflammation and Cancer. *Nature* **2002**, *420*, 860–867.
- (11) Wellen, K. E.; Hotamisligil, G. S. Inflammation, Stress, and Diabetes. *J. Clin. Invest.* **2005**, *115*, 1111–1119.
- (12) Schroder, K.; Tschopp, J. The Inflammasomes. *Cell* **2010**, *140*, 821–832.
- (13) Martinon, F.; Burns, K.; Tschopp, J. The Inflammasome: A Molecular Platform Triggering Activation of Inflammatory Caspases and Processing of proIL-B. *Mol. Cell* **2002**, *10*, 417–426.
- (14) Hornung, V.; Ablasser, A.; Charrel-Dennis, M.; Bauernfeind, F.; Horvath, G.; Caffrey, D. R.; Latz, E.; Fitzgerald, K. A. AIM2 Recognizes Cytosolic dsDNA and Forms a Caspase-1-Activating Inflammasome with ASC. *Nature* **2009**, *458*, 514–518.
- (15) Fernandes-Alnemri, T.; Yu, J.; Datta, P.; Wu, J.; Alnemri, E. AIM2 Activates the Inflammasome and Cell Death in Response to Cytoplasmic DNA. *Nature* **2009**, *458*, 509–513.
- (16) Yu, J.-W.; Wu, J.; Zhang, Z.; Datta, P.; Ibrahim, I.; Taniguchi, S.; Sagara, J.; Fernandes-Alnemri, T.; Alnemri, E. S. Cryopyrin and Pyrin Activate Caspase-1, but Not NF- κ B, via ASC Oligomerization. *Cell Death Differ.* **2006**, *13*, 236–249.
- (17) Mariathasan, S.; Newton, K.; Monack, D. M.; Vucic, D.; French, D. M.; Lee, W. P.; Roose-Girma, M.; Erickson, S.; Dixit, V. M.

Differential Activation of the Inflammasome by Caspase-1 Adaptors ASC and Ipaf. *Nature* **2004**, *430*, 213–218.

(18) Hornung, V.; Latz, E. Critical Functions of Priming and Lysosomal Damage for NLRP3 Activation. *Eur. J. Immunol.* **2010**, *40*, 620–623.

(19) Beutler, B. Tlr4: Central Component of the Sole Mammalian LPS Sensor. *Curr. Opin. Immunol.* **2000**, *12*, 20–26.

(20) Lu, Y. C.; Yeh, W. C.; Ohashi, P. S. LPS/TLR4 Signal Transduction Pathway. *Cytokine+* **2008**, *42*, 145–151.

(21) Libermann, T. A.; Baltimore, D. Activation of Interleukin-6 Gene Expression through the NF-Kappa B Transcription Factor. *Mol. Cell. Biol.* **1990**, *10*, 2327–2334.

(22) Cogswell, J. P.; Godlevski, M. M.; Wisely, C. B.; Leesnitzer, L. M.; Ways, J. P.; Gray, J. G.; Clay, C. NF-Kappa B Regulates IL-1 Beta Transcription through a Consensus NF-Kappa B Binding Site and a Nonconsensus CRE-like Site. *J. Immunol.* **1994**, *153*, 712–723.

(23) Liu, H.; Sidiropoulos, P.; Song, G.; Pagliari, L. J.; Birrer, M. J.; Stein, B.; Anrather, J.; Pope, R. M. TNF-A Gene Expression in Macrophages: Regulation by NF- κ B Is Independent of c-Jun or C/EBP. *J. Immunol.* **2000**, *164*, 4277–4285.

(24) Bauernfeind, F. G.; Horvath, G.; Stutz, A.; Alnemri, E. S.; MacDonald, K.; Speert, D.; Fernandes-Alnemri, T.; Wu, J.; Monks, B. G.; Fitzgerald, K. A.; Hornung, V.; Latz, E. Cutting Edge: NF-kappaB Activating Pattern Recognition and Cytokine Receptors License NLRP3 Inflammasome Activation by Regulating NLRP3 Expression. *J. Immunol.* **2009**, *183*, 787–791.

(25) Juliana, C.; Fernandes-Alnemri, T.; Kang, S.; Farias, A.; Qin, F.; Alnemri, E. S. Non-Transcriptional Priming and Deubiquitination Regulate NLRP3 Inflammasome Activation. *J. Biol. Chem.* **2012**, *287*, 36617–36622.

(26) Py, B. F.; Kim, M. S.; Vakifahmetoglu-Norberg, H.; Yuan, J. Deubiquitination of NLRP3 by BRCC3 Critically Regulates Inflammasome Activity. *Mol. Cell* **2013**, *49*, 331–338.

(27) Song, N.; Liu, Z. S.; Xue, W.; Bai, Z. F.; Wang, Q. Y.; Dai, J.; Liu, X.; Huang, Y. J.; Cai, H.; Zhan, X. Y.; Han, Q. Y.; Wang, H.; Chen, Y.; Li, H. Y.; Li, A. L.; Zhang, X. M.; Zhou, T.; Li, T. NLRP3 Phosphorylation Is an Essential Priming Event for Inflammasome Activation. *Mol. Cell* **2017**, *68*, 185–197.e6.

(28) Lopez-Castejon, G.; Loheshi, N. M.; Compan, V.; High, S.; Whitehead, R. C.; Flitsch, S.; Kirov, A.; Prudovsky, I.; Swanton, E.; Brough, D. Deubiquitinases Regulate the Activity of Caspase-1 and Interleukin-1 β Secretion via Assembly of the Inflammasome. *J. Biol. Chem.* **2013**, *288*, 2721–2733.

(29) Martinon, F.; Petrilli, V.; Mayor, A.; Tardivel, A.; Tschopp, J. Gout-Associated Uric Acid Crystals Activate the NALP3 Inflammasome. *Nature* **2006**, *440*, 237–241.

(30) Pelegrin, P.; Surprenant, A. Pannexin-1 Mediates Large Pore Formation and Interleukin-1beta Release by the ATP-Gated P2 \times 7 Receptor. *EMBO J.* **2006**, *25*, S071–S082.

(31) Halle, A.; Hornung, V.; Petzold, G. C.; Stewart, C. R.; Monks, B. G.; Reinheckel, T.; Fitzgerald, K. A.; Latz, E.; Moore, K. J.; Golenbock, D. T. The NALP3 Inflammasome Is Involved in the Innate Immune Response to Amyloid-Beta. *Nat. Immunol.* **2008**, *9*, 857–865.

(32) Lu, A.; Magupalli, V.; Ruan, J.; Yin, Q.; Atianand, M. K.; Vos, M.; Schröder, G. F.; Fitzgerald, K. A.; Wu, H.; Egelman, E. H. Unified Polymerization Mechanism for the Assembly of ASC-Dependent Inflammasomes. *Cell* **2014**, *156*, 1193–1206.

(33) Brough, D.; Rothwell, N. J. Caspase-1-Dependent Processing of pro-Interleukin-1 β Is Cytosolic and Precedes Cell Death. *J. Cell Sci.* **2007**, *120*, 772–781.

(34) Martin-Sanchez, F.; Diamond, C.; Zeitler, M.; Gomez, A. I.; Baroja-Mazo, A.; Bagnall, J.; Spiller, D.; White, M.; Daniels, M. J. D.; Mortellaro, A.; Penalver, M.; Paszek, P.; Steringer, J. P.; Nickel, W.; Brough, D.; Pelegrin, P. Inflammasome-Dependent IL-1 β Release Depends upon Membrane Permeabilisation. *Cell Death Differ.* **2016**, *23*, 1219–1231.

(35) Brough, D.; Pelegrin, P.; Nickel, W. An Emerging Case for Membrane Pore Formation as a Common Mechanism for the

Unconventional Secretion of FGF2 and IL-1 β . *J. Cell Sci.* **2017**, *130*, 3197–3202.

(36) Rodrigues, A. F.; Newman, L.; Lozano, N.; Mukherjee, S. P.; Fadeel, B.; Bussy, C.; Kostarelos, K. A Blueprint for the Synthesis and Characterisation of Thin Graphene Oxide with Controlled Lateral Dimensions for Biomedicine. *2D Mater.* **2018**, *5*, 035020.

(37) Mukherjee, S. P.; Lozano, N.; Kucki, M.; Del Rio-Castillo, A. E.; Newman, L.; Vazquez, E.; Kostarelos, K.; Wick, P.; Fadeel, B. Detection of Endotoxin Contamination of Graphene Based Materials Using the TNF-A Expression Test and Guidelines for Endotoxin-Free Graphene Oxide Production. *PLoS One* **2016**, *11*, e0166816.

(38) Pinteaux, E.; Parker, L. C.; Rothwell, N. J.; Loheshi, G. N. Expression of Interleukin-1 Receptors and Their Role in Interleukin-1 Actions in Murine Microglial Cells. *J. Neurochem.* **2002**, *83*, 754–763.

(39) Daniels, M. J. D.; Rivers-Auty, J.; Schilling, T.; Spencer, N. G.; Watremez, W.; Fasolino, V.; Booth, S. J.; White, C. S.; Baldwin, A. G.; Freeman, S.; Wong, R.; Latta, C.; Yu, S.; Jackson, J.; Fischer, N.; Koziel, V.; Pillot, T.; Bagnall, J.; Allan, S. M.; et al. Fenamate NSAIDs Inhibit the NLRP3 Inflammasome and Protect against Alzheimer's Disease in Rodent Models. *Nat. Commun.* **2016**, *7*, 12504.

(40) Coll, R. C.; Robertson, A. A.; Chae, J. J.; Higgins, S. C.; Muñoz-Planillo, R.; Inerra, M. C.; Vetter, I.; Dungan, L. S.; Monks, B. G.; Stutz, A.; Croker, D. E.; Butler, M. S.; Haneklaus, M.; Sutton, C. E.; Nuñez, G.; Latz, E.; Kastner, D. L.; Mills, K. H.; Masters, S. L.; et al. A Small Molecule Inhibitor of the NLRP3 Inflammasome for the Treatment of Inflammatory Diseases. *Nat. Med.* **2015**, *21*, 248–255.

(41) Vranic, S.; Rodrigues, A. F.; Buggio, M.; Newman, L.; White, M. R. H.; Spiller, D. G.; Bussy, C.; Kostarelos, K. Live Imaging of Label-Free Graphene Oxide Reveals Critical Factors Causing Oxidative Stress-Mediated Cellular Responses. *ACS Nano* **2018**, *12*, 1373–1389.

(42) Bambouskova, M.; Gorvel, L.; Lampropoulou, V.; Sergushichev, A.; Loginicheva, E.; Johnson, K.; Korenfeld, D.; Mathyer, M. E.; Kim, H.; Huang, L. H.; Duncan, D.; Bregman, H.; Keskin, A.; Santeford, A.; Apte, R. S.; Sehgal, R.; Johnson, B.; Amarasinghe, G. K.; Soares, M. P.; et al. Electrophilic Properties of Itaconate and Derivatives Regulate the I κ B ζ -ATF3 Inflammatory Axis. *Nature* **2018**, *556* (7702), 501–504.

(43) Mills, E. L.; Ryan, D. G.; Prag, H. a.; Dikovskaya, D.; Menon, D.; Zaslona, Z.; Jedrychowski, M. P.; Costa, A. S. H.; Higgins, M.; Hams, E.; Szpyt, J.; Runtsch, M. C.; King, M. S.; McGouran, J. F.; Fischer, R.; Kessler, B. M.; McGettrick, A. F.; Hughes, M. M.; Carroll, R. G.; et al. Itaconate Is an Anti-Inflammatory Metabolite That Activates Nrf2 via Alkylation of KEAP1. *Nature* **2018**, *556*, 113–117.

(44) Kobayashi, E. H.; Suzuki, T.; Funayama, R.; Nagashima, T.; Hayashi, M.; Sekine, H.; Tanaka, N.; Moriguchi, T.; Motohashi, H.; Nakayama, K.; Yamamoto, M. Nrf2 Suppresses Macrophage Inflammatory Response by Blocking Proinflammatory Cytokine Transcription. *Nat. Commun.* **2016**, *7*, 11624.

(45) Chen, H.-T.; Wu, H.-Y.; Shih, C.-H.; Jan, T.-R. A Differential Effect of Graphene Oxide on the Production of Proinflammatory Cytokines by Murine Microglia. *Taiwan Shouyixue Zazhi* **2015**, *41*, 205–211.

(46) Chiacchiaretta, M.; Bramini, M.; Rocchi, A.; Armirotti, A.; Giordano, E.; Vázquez, E.; Bandiera, T.; Ferroni, S.; Cesca, F.; Benfenati, F. Graphene Oxide Upregulates the Homeostatic Functions of Primary Astrocytes and Modulates Astrocyte-to-Neuron Communication. *Nano Lett.* **2018**, *18*, 5827–5838.

(47) Ma, J.; Liu, R.; Wang, X.; Liu, Q.; Chen, Y.; Valle, R. P.; Zuo, Y.; Xia, T.; Liu, S. Crucial Role of Lateral Size for Graphene Oxide in Activating Macrophages and Stimulating Pro-Inflammatory Responses in Cells and Animals. *ACS Nano* **2015**, *9*, 10498–10515.

(48) Russier, J.; Treossi, E.; Scarsi, A.; Perrozzini, F.; Dumortier, H.; Ottaviano, L.; Meneghetti, M.; Palermo, V.; Bianco, A. Evidencing the Mask Effect of Graphene Oxide: A Comparative Study on Primary Human and Murine Phagocytic Cells. *Nanoscale* **2013**, *5*, 11234.

(49) Yue, H.; Wei, W.; Yue, Z.; Wang, B.; Luo, N.; Gao, Y.; Ma, D.; Ma, G.; Su, Z. The Role of the Lateral Dimension of Graphene Oxide

in the Regulation of Cellular Responses. *Biomaterials* **2012**, *33*, 4013–4021.

(50) Orecchioni, M.; Jasim, D.; Pescatori, M.; Sgarrella, F.; Bedognetti, D.; Bianco, A.; Kostarelos, K.; Delogu, L. Molecular Impact of Graphene Oxide with Different Shape Dimension on Human Immune Cells. *J. Immunother. Cancer* **2015**, *3*, P217.

(51) Chen, G. Y.; Yang, H. J.; Lu, C. H.; Chao, Y. C.; Hwang, S. M.; Chen, C. L.; Lo, K. W.; Sung, L. Y.; Luo, W. Y.; Tuan, H. Y.; Hu, Y. C. Simultaneous Induction of Autophagy and Toll-like Receptor Signaling Pathways by Graphene Oxide. *Biomaterials* **2012**, *33*, 6559–6569.

(52) Wang, X.; Duch, M. C.; Mansukhani, N.; Ji, Z.; Liao, Y. P.; Wang, M.; Zhang, H.; Sun, B.; Chang, C. H.; Li, R.; Lin, S.; Meng, H.; Xia, T.; Hersam, M. C.; Nel, A. E. Use of a Pro-Fibrogenic Mechanism-Based Predictive Toxicological Approach for Tiered Testing and Decision Analysis of Carbonaceous Nanomaterials. *ACS Nano* **2015**, *9*, 3032–3043.

(53) Mukherjee, S. P.; Kostarelos, K.; Fadeel, B. Cytokine Profiling of Primary Human Macrophages Exposed to Endotoxin-Free Graphene Oxide: Size-Independent NLRP3 Inflammasome Activation. *Adv. Healthcare Mater.* **2018**, *7*, 1700815.

(54) Hornung, V.; Bauernfeind, F.; Halle, A.; Samstad, E. O.; Kono, H.; Rock, K. L.; Fitzgerald, K. A.; Latz, E. Silica Crystals and Aluminum Salts Activate the NALP3 Inflammasome through Phagosomal Destabilization. *Nat. Immunol.* **2008**, *9*, 847–856.

(55) Dostert, C.; Pétrilli, V.; Van Bruggen, R.; Steele, C.; Mossman, B. T.; Tschopp, J. Innate Immune Activation Through Nalp3 Inflammasome Sensing of Asbestos and Silica. *Science* **2008**, *320*, 674–677.

(56) Zhang, B.; Wei, P.; Zhou, Z.; Wei, T. Interactions of Graphene with Mammalian Cells: Molecular Mechanisms and Biomedical Insights. *Adv. Drug Delivery Rev.* **2016**, *105*, 145–162.

(57) Ali-Boucetta, H.; Bitounis, D.; Raveendran-Nair, R.; Servant, A.; Van den Bossche, J.; Kostarelos, K. Purified Graphene Oxide Dispersions Lack *In Vitro* Cytotoxicity and *In Vivo* Pathogenicity. *Adv. Healthcare Mater.* **2013**, *2*, 433–441.

(58) Jasim, D.; Lozano, N.; Kostarelos, K. Synthesis of Few-Layered, High-Purity Graphene Oxide Sheets from Different Graphite Sources for Biology. *2D Mater.* **2016**, *3*, 014006.

(59) Love, M. I.; Huber, W.; Anders, S. Moderated Estimation of Fold Change and Dispersion for RNA-Seq Data with DESeq2. *Genome Biol.* **2014**, *15*, 550.

(60) R Core Team. *R: A Language and Environment for Statistical Computing*. R Foundation for Statistical Computing, Vienna, Austria. ISBN 3-900051-07-0; <http://www.R-project.org/> 2018. DOI: DOI: 10.1007/978-3-540-74686-7.

(61) Chen, E. Y.; Tan, C. M.; Kou, Y.; Duan, Q.; Wang, Z.; Meirelles, G. V.; Clark, N. R.; Ma'ayan, A. Enrichr: Interactive and Collaborative HTML5 Gene List Enrichment Analysis Tool. *BMC Bioinf.* **2013**, *14*, 128.

(62) Kuleshov, M. V.; Jones, M. R.; Rouillard, A. D.; Fernandez, N. F.; Duan, Q.; Wang, Z.; Koplev, S.; Jenkins, S. L.; Jagodnik, K. M.; Lachmann, A.; McDermott, M. G.; Monteiro, C. D.; Gundersen, G. W.; Ma'ayan, A. Enrichr: A Comprehensive Gene Set Enrichment Analysis Web Server 2016 Update. *Nucleic Acids Res.* **2016**, *44* (W1), W90–W97.